DUCTILITY ASSESSMENT OF REINFORCED CONCRETE PILE-TO-PILE CAP CONNECTIONS IN APPLICATION

Mochamad Teguh
Lecturer at the Department of Civil Engineering,
Faculty of Civil Engineering and Planning, Islamic University of Indonesia
Integrated Campus, Jl. Kaliurang Km 14,5, Yogyakarta 55584
e-mail: m.teguh@ftsp.uii.ac.id

ABSTRACT

Ground motion occurred during moderate seismic event causes pile-to-pile cap connections producing a large curvature demand and a plastic hinge at the pile head. Severity damage along the pile is controlled by limiting the curvature ductility demand in the potential plastic hinge region of the pile. The strength and stiffness of the soil-pile interaction and the equivalent plastic hinge length of the pile directly quantify the curvature ductility demand of fixed pile-to-pile cap connection. A routine that incorporates the limit state analysis based on the kinematic model and the moment-curvature analysis was developed to calculate the displacement ductility factor to the local curvature ductility demand. A fixed-head pile-to-pile cap connection embedded in cohesive and cohesionless soils was studied. The result shows that the first plastic hinges for both soil conditions occur at the interface of fixed-head pile connection. The ductility assessment demonstrates that curvature ductility demands for the fixed-head pile embedded in cohesive soil is higher compared to the pile embedded in cohesionless soil providing a different location of the second plastic hinges.

Keywords: curvature demand, ductility demand, plastic hinge, fixed-head, pile-to-pile cap connection

INTRODUCTION

Previous seismic design practice of the pile foundations has commonly simplified the effect of the ground motions applied to the structure, particularly in the design of pile-to-pile cap connections. This concept is generally a conservative design assumption for a spectral analysis approach, as the flexible pile foundation results in period lengthening and increased damping, and consequent decreased structural forces relative to a fixed base case. In extreme cases, such as the 1985 Mexico City Earthquake, however, period lengthening causes increased spectral values in relation to the current code specifications recommended by the National Earthquake Hazards Reduction Program (NEHRP) (Holmes, 2000). Seismic behavior of the pile-to-pile cap connections depends on the ductility capacity of its yielding members. In the case of reinforced concrete piles, the overall ductility capacity of the structure is dependent on the local ductility capacity of the pile, which should be adequately confined to ascertain a ductile behavior. In addition, amount of reinforcement details of longitudinal and confinement and the compressive strength of concrete directly affect to the lateral stiffness, strength, and ductility capacity of the pile. Consequently, the lateral force-deformation characteristics of the pile also depend on the interaction between the pile and surrounding soil.

The analyses described in the present study were carried out to provide a better definition of the ductility capacity and to specifically identify the parameters affecting equivalent plastic hinge length, depth to equivalent fixity for displacement, and depth to position of maximum moment. A soil with stiffness increasing linearly with depth (typically for a granular soil) was assumed. The lateral loading of pile acting on the pile cap produces different moment patterns depending on either free-head or fixed-head piles. The controlling hinge in a fixed-head pile will develop at the pile-to-pile cap connection; attainment of the full inelastic potential of this hinge will generally result in the formation of a second, subgrade hinge (Budek et al., 2000).

In this study, only a fixed-head pile was then considered in the analysis of pile-to-pile cap connections where the headed reinforcement confined with spiral reinforcement has been taken into account. In fact, the state of current practice shows that fixed-head piles are more typically used in pile groups where the response of an individual pile can be influenced through the adjacent soil by the response of nearby piles.

MODEL DESCRIPTION OF LATERALLY LOADED PILE: FIXED-HEAD CASE

An analytical model of laterally loaded pile was applied to the fixed-head pile-to-pile cap connections embedded in cohesive and cohesionless soils as depicted in Figure 1. According to NEHRP (2001), soil profiles of the two soil conditions are classified as cohesive soil and cohesionless soil. In this study, a single reinforced concrete pile-to-pile cap connection is fully embedded in the soil to analyze ductility assessment of the structure. Fixity of the pile head against rotation was considered. The pile has a diameter of D = 1.83 m and an embedded length of 33 m, as shown in Figure 1a. The pile as presented in Figure 1b was reinforced with 32 longitudinal reinforcements of 43 mm diameter and confined with spiral reinforcement of 19 mm diameter and 110 mm spiral pitch. Compressive strength of 27.6 MPa and an axial load compression of 7259 kN or 0.1 $A_c.f_c'$ was assumed. Probable yield strength of rebar was assumed to be 455 MPa, 10% above normal grade value. Material and section properties of the pile used in this analysis are listed in Table 1.

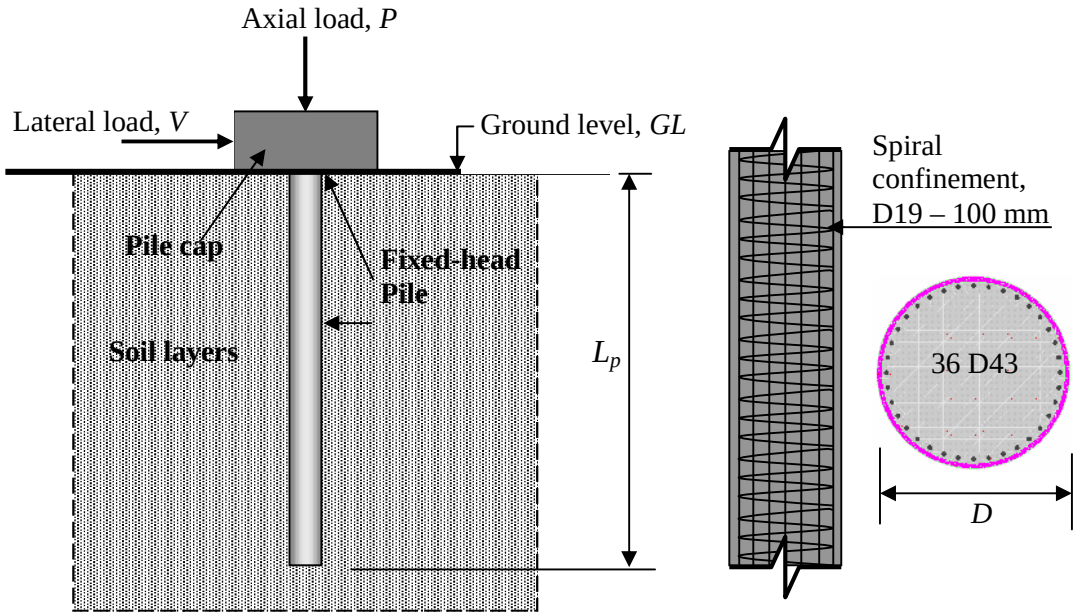

(a) Detail of fixed-head pile (b) Circular pile cross-section

Figure 1. Winkler beam model of soil-pile system

Table 1. Material and section properties of reinforced concrete pile

Material description	Quantity
Pile diameter, D	1.83 m
Concrete cover	50.4 mm
Compressive strength of concrete, f_c'	27.6 MPa
Expected compressive strength of concrete, $f_{ce}' = 1.3 f_c'$	35.9 MPa
Tensile strength	- 1.9 MPa
Yield strain	3.5×10^{-3}
Unconfined crushing strain	4.0×10^{-3}
Confined crushing strain	14.6×10^{-3}
Spalling strain	6.0×10^{-3}
Concrete elastic modulus, E_c	24870 MPa
Confined concrete strength	35.9 MPa
Longitudinal reinforcement	36 D43

Lanjutan Tabel-1:

Spiral reinforcement and pitch	D19 – 110 mm
Yield strength of longitudinal and spiral steel, f_y	455 MPa
Expected yield strength of longitudinal and spiral steel, $f_{ye} = 1.13\ f_y$	514.2 MPa
Embedded pile length, L_d	33.0 m
Moment of inertia ($I_x = I_y$)	5.6×10^{11} mm^4
Longitudinal reinforcement ratio, ρ_l	1.99%
Transversal spiral reinforcement ratio, ρ_s	0.6 %
Unconfined area of concrete	281.6×10^3 mm^2
Confined area of concrete	2.3×10^6 mm^2
Axial force, $P = 0.1\ A_c\ f_c'$	7259 kN

MOMENT-CURVATURE ANALYSIS

Moment-curvature analysis is essentially required to define a sectional capacity of the reinforced concrete pile, such as the moment-curvature relationship at yield and ultimate conditions. A nonlinear sectional analysis using the XTRACT source code (Chadwell and Imbsen, 2004) was carried out to determine equivalent elastoplastic yield and ultimate curvatures to satisfy seismic performance of a structure, as the damage can be controlled by limiting the strain values in critical regions.

To start with, the concrete pile section was discretised into small triangular elements to cover confined and unconfined concrete areas in determining accurate confined concrete strength and crushing strain. As a comparison, a reinforced concrete pile modeled by Budek et al. (2000) was selected in the application as presented in this section. Table 1 shows material and section properties of a reinforced concrete pile used in the analysis of laterally loaded piles.

The modified Scott Model was utilized to compute the stress and strain of confined concrete. The unconfined and confined stress-strain relationships are shown in Figure 2, while the stress-strain relationship of longitudinal and transverse spiral steels is presented in Figure 3. Due to the circular cross-section of the pile and symmetric longitudinal steels, only the moment-curvature about the *x* axis was computed.

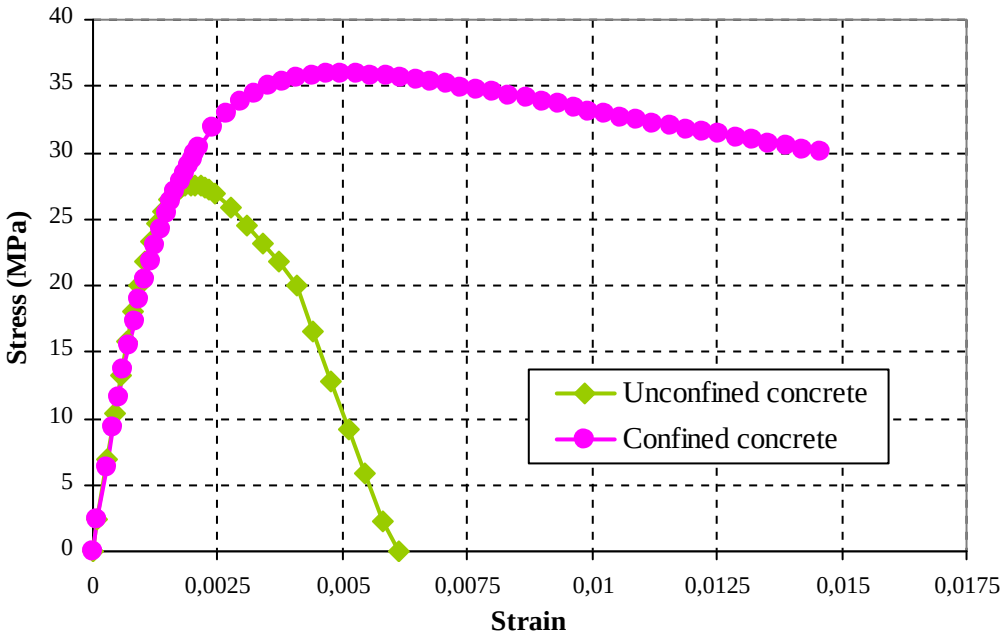

Figure 2. Stress-strain relationships for reinforced concrete pile

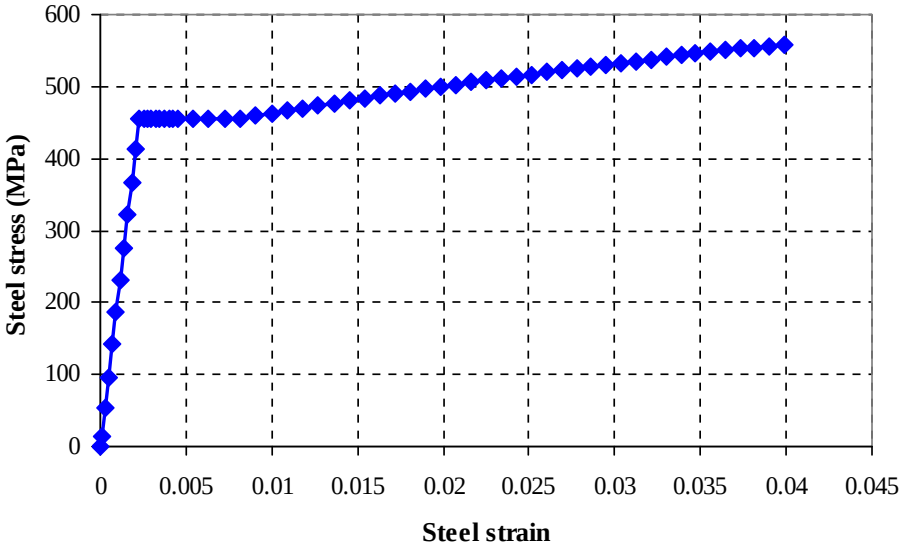

Figure 3. Stress-strain relationships for longitudinal and spiral reinforcement

Two interaction models were performed in this analysis, i.e. axial force moment interaction and moment-curvature interaction. In the first interaction model, limiting strains for both concrete and steel materials were specified and the reduction factor for moment and axial load was varied from 0.7 to 0.9, with maximum axial capacity set equal to 0.56 $A_g.f_c'$. For the second interaction model, the first step load applied was provided equal to 0.1 $A_g.f_c'$ and the load was incremented at moment about the x axis (M_{xx}). The plastic hinge length was assumed as 915 mm, which is equal to half the pile diameter, to calculate the moment rotation. The confined concrete model was reduced to incorporate the effects of concrete arching action (Paulay and Priestley, 1992). Figure 4a shows a discretised cross-section for the undeformed condition and Figure 4b presents a deformed cross-section at the ultimate load, with the bottom in compression about the x axis. Figure 4b shows an image of the deformed cross-section that has experienced such deformations. The blue fibers illustrate the confined concrete in compression, the white fibers represent unconfined cover concrete that has spalled off, and the green bars symbolize longitudinal reinforcement in the strain-hardening regime.

The moment-curvature analysis results presented in Figure 5 and Table 2 show good agreement; which is achieved when the moment-curvature computed with the sectional technique is compared with theoretical analysis proposed by Budek et al. (2000). In this analysis, the confined model used the Modified Scott model while Budek et al. (2000) have used the Mander model (Mander et al., 1988). When the reinforcement starts yielding at the inelastic condition, the Mander model has shown a more conservative moment-curvature compared with the Modified Scott model; however, the results have satisfied the theoretical stress-strain relationships.

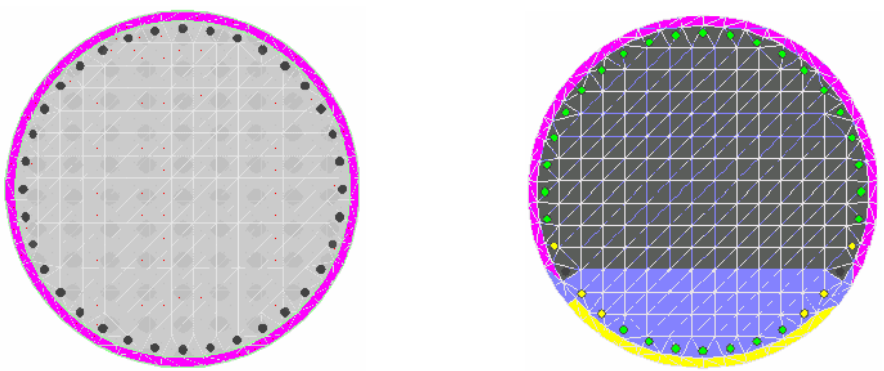

(a) Undeformed cross-section (b) Deformed cross-section

Figure 4. Discretised pile cross-section

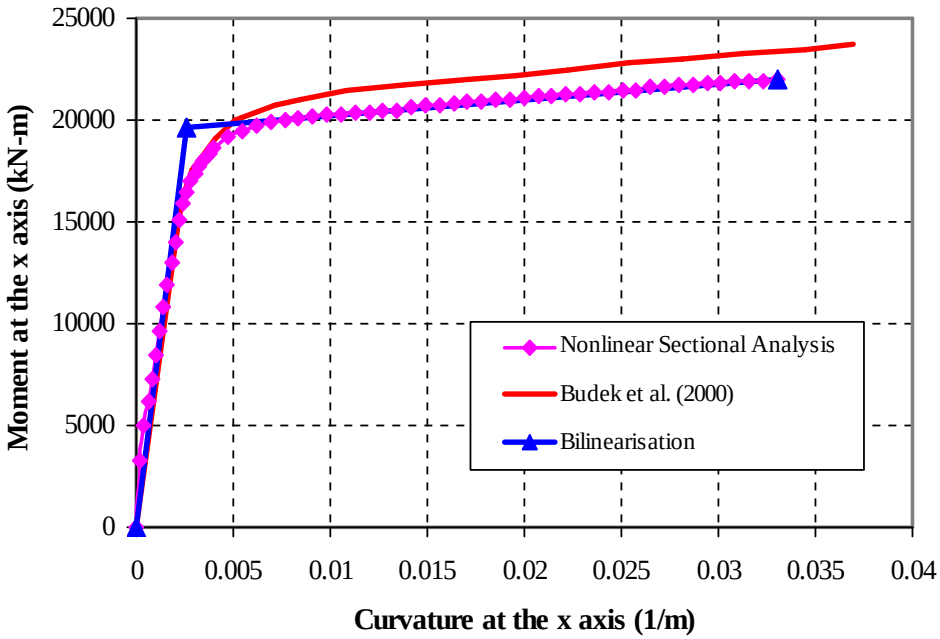

Figure 5. Moment-curvature relationships for the circular reinforced concrete pile

The axial force moment interaction was used as an alternative to calculate the axial force-ultimate curvature relation. The purpose of this interaction is to perform a sequence of moment-curvature analyses with differing axial forces. In this case, a moment-curvature analysis is only performed with the axial force of 0.1 $A_g.f_c'$ applied to the confined concrete cross-section shown in Figure 6. More details on a combination of the moment-curvature for different parameters, such as different axial forces, pile cross-sections, and reinforcement ratios, are described in Teguh (2007).

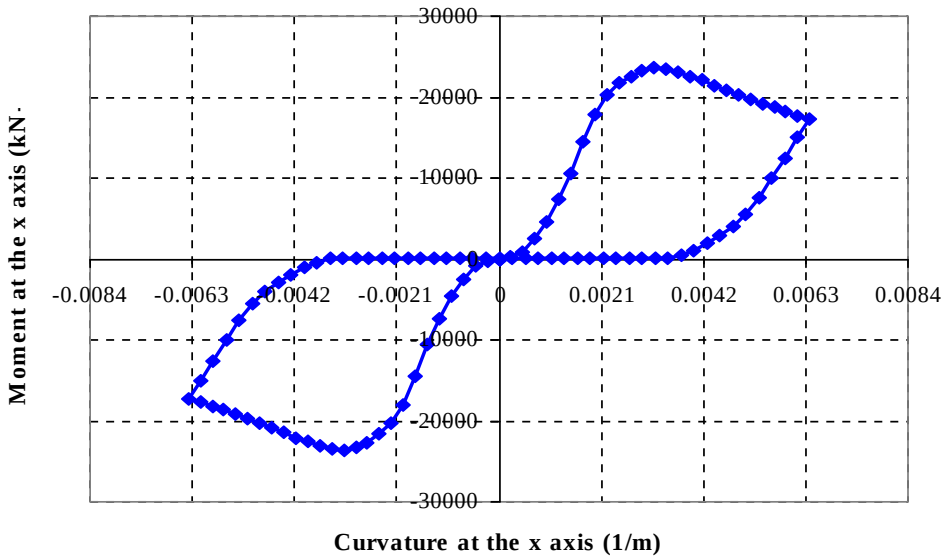

Figure 6. Moment-curvature relationship at the x axis

Table 2. Pile analysis results

Description	First yield	Ultimate
Moment at about *x* axis, M_{xx}	1.4×10^4 kN-m	2.2×10^4 kN-m
Curvature, ϕ	2.0×10^{-3} 1/m	33.0×10^{-3} 1/m
Effective moment	1.97×10^4	kN-m
Effective curvature	2.8×10^{-3}	1/m
Curvature ductility	11.7	
Over strength factor	1.1	
Plastic rotation capacity	27.7×10^{-3}	rad
Bilinear hardening slope	1.1	%

RESULTS AND DISCUSSION ON LIMIT STATE ANALYSIS

An application of the limit state analysis is to analyze deep pile foundations with fixed pile-to-pile cap connections subjected to a large curvature demand at the pile head or pile cap. Under seismic events, pile damage induced by local inelastic deformation depends on the magnitude of the lateral displacement imposed on the pile.

In this application, a single reinforced concrete pile-to-pile cap connection shown in Figure 1 is considered as a floating pile embedded in cohesive and cohesionless soils. With regard to the reinforced concrete material, the ATC-32 (1996) suggested that the expected compressive strength of concrete is $f_{ce}^{'} = 1.3 f_c^{'} =$ 35.9 MPa. Caltrans (2001) has recommended that the expected yield strength of steel is f_{ye} = 1.13 f_y = 514.12 MPa. Both soil profiles have been classified referring to the NEHRP (2001) recommendations as depicted in Table 3. For estimation of curvature ductility demand, the soil stiffness should correspond to the first yield limit state and it should be strictly reduced, as softening of the soil would have occurred upon first yielding of the pile.

The moment-curvature response of the pile section was idealized by an elastoplastic response as shown in Figure 5. To meet seismic performance of the pile foundation system, the pile damage was controlled by limiting the strain values in the critical regions. Kowalsky (2000) suggested a damage control strain of 0.018 for the extreme fiber of the confined concrete core, or 0.060 for the extreme tension fiber of longitudinal reinforcement. Following this suggestion for the damage control for fixed-head piles, the limiting curvature of the pile is $\phi_u = 0.03304$ rad/m considered as the ultimate curvature of the section (Table 1). Providing the level of confining steel for the pile, the curvature ductility capacity is $(\mu_\phi)_{cap} = 11.72$ and the curvature ductility demand was estimated for a range up to 3 of an imposed displacement ductility factor.

Referring to the analytical approach presented in a companion paper, both kinematic relations for first and second plastic hinges were calculated and the results are then plotted in Figure 7 and Figure 8. The resulting kinematic relations show that the curvature ductility factor increases linearly with the displacement ductility factor for both plastic hinges, however both straight lines of first and second plastic hinges are not parallel. In the small displacement range, where only one plastic hinge forms, i.e. μ_Δ < 1.47, the slope of the line is also slightly different from the slope where two plastic hinges form. For a curvature ductility capacity of 11.72, as estimated for the pile section, the result in Figure 7 indicates that the fixed-head pile can tolerate a displacement ductility factor of 1.63. For a displacement ductility factor of μ_Δ = 1, the curvature ductility demand in the first plastic hinge is $\mu_{\phi 1} = 5.19$. The reason for the curvature ductility factor greater than unity is due to the definition of the elasto-plastic yield displacement Δ_y = 0.2335 m, which is larger than the lateral displacement to cause the first yield of the pile Δ_{y1} = 0.123 m.

The resulting kinematic relations are plotted in Figure 8 for comparison with the case of soft clay. The curvature ductility demand for the pile in dense sand follows the same trend as that of the soft clay, with a linearly increasing curvature ductility factor for an increased displacement ductility factor. For a given displacement ductility factor, however, the curvature ductility demand in dense sand is significantly smaller than the curvature ductility demand in soft clay. For example, at a displacement ductility factor of μ_Δ = 3, the curvature ductility demand is $\mu_{\phi 1} = 7.41$ for the case of dense sand compared to the curvature ductility demand of $\mu_{\phi 1} = 26.1$ for soft clay.

Table 3. Soil properties according to NEHRP (2001)

Description	Cohesive soil	Cohesionless soil
NEHRP soil classification, soil profile	Class E site, S_E (soft clay)	Class C site, S_C (dense sand)
Undrained shear strength, S_u	35.0 kPa	-
Friction angle, $\bar{\phi}$	-	42^0
Effective weight of soil, γ'	17.5 kN/m^3	20.5 kN/m^3

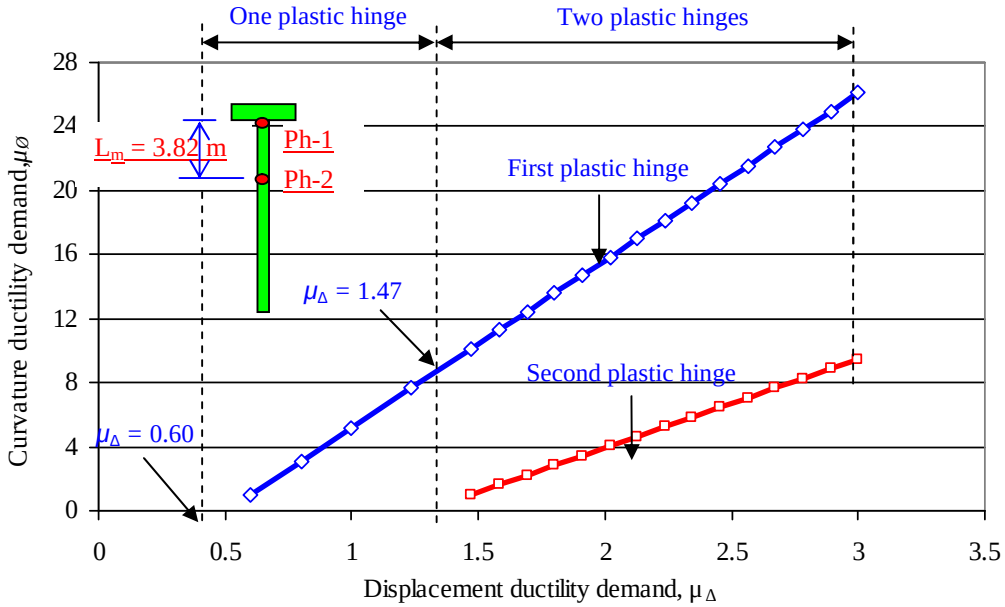

Figure 7. Kinematic relation for a fixed-head pile embedded in cohesive soil

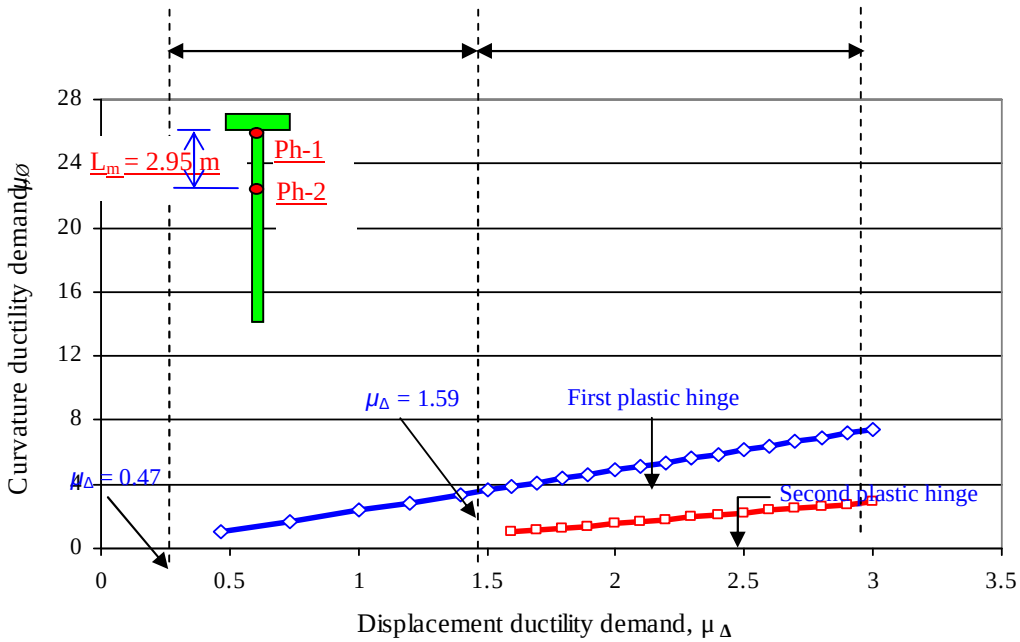

Figure 8. Kinematic relation for a fixed-head pile embedded in cohesionless soil

CONCLUDING REMARKS

The following concluding remarks are drawn based on the theoretical development presented in a companion paper and its numerical applications.

1. The resulting kinematic relations for cohesive soil show that the curvature ductility factor increases linearly with the displacement ductility factor for both plastic hinges; however, both straight lines of first and second plastic hinges are not parallel. In the small displacement range where only one plastic hinge forms, i.e. $\mu_\Delta < 1.47$, the slope of the line is also slightly different from the slope where two plastic hinges form. For a curvature ductility capacity of 11.72 as estimated for the pile section, the result in Figure 7 indicates that the fixed-head pile can tolerate a displacement ductility factor of 1.63.
2. The curvature ductility demand for the pile in dense sand follows the same trend as in soft clay, with a linearly increasing curvature ductility factor for an increased displacement ductility factor. For a given displacement ductility factor, however, the curvature ductility demand in dense sand is significantly smaller than the curvature ductility demand in soft clay. As seen in the application, at a displacement ductility factor of $\mu_\Delta = 3$, the curvature ductility demand is $\mu_{\phi 1} = 7.41$ for the case of dense sand compared to the curvature ductility demand of $\mu_{\phi 1} = 26.1$ for soft clay. Although it was not plotted in Figure 8, the estimated curvature ductility capacity of 11.72 for the pile section would correspond to a displacement ductility factor of $\mu_\Delta = 4.70$.
3. Advanced studies on laterally loaded piles applied to free-head and fixed-head cases that are embedded partially and fully in different soil profiles are highly recommended to enhance seismic performance of the pile-to-pile cap connections.

REFERENCES

ATC-32., 1996, *Improved Seismic Design Criteria for California Bridges: Provisional Recommendations*, Redwood City, California.

Budek, A. M., Priestley, M. J. N., and Benzoni, G., 2000, Inelastic Seismic Response of Bridge Drilled-Shaft RC Pile/Column, *Journal of Structural Engineering, ASCE*, V. 126(Issue 4), 510-517.

Caltrans, 2001, *Caltrans Seismic Design Criteria, Version 1.2.*, California Department of Transportation, Sacramento, California.

Chadwell, C. B., and Imbsen, R. A., 2004, XTRACT - Cross Section Analysis Software for Structural and Earthquake Engineering, *http://www.imbsen.com/xtract.htm*.

Holmes, W. T., 2000, The 1997 NEHRP Recommended Provisions for Seismic Regulations for New Building and Other Structures, *Earthquake Spectra*, Vol. 16, No. 1, pp. 101-114.

Kowalsky, M. J., 2000, Deformation Limit States for Circular Reinforced Concrete Bridge Columns, *Journal of Structural Engineering, ASCE*, Vol. 126, No. 8, pp. 869-878.

Mander, J. B., Priestley, M. J. N., and Park, R., 1988, Theoretical Stress-Strain Model for Confined Concrete, *Journal of Structural Engineering, ASCE*, V.114, 1804-1826.

NEHRP, 2001, *NEHRP Recommended Provisions for Seismic Regulations for New Buildings and Other Structures, FEMA 368*, Washington, D.C.

Paulay, T., and Priestley, M. J. N., 1992, *Seismic Design of Reinforced Concrete and Masonry Buildings*, Wiley, New York.

Teguh, M., 2007, Seismic Performance of Prestressed Concrete Pile-to-pile Cap Connections, *Ph.D Thesis*, Department of Civil and Environmental Engineering, University of Melbourne, Australia.